Journal of Guidance, Control, and Dynamics
Vol. 38, No. 5, May 2015

Probabilistic Assessment of Lifetime of Low-Earth-Orbit Spacecraft: Uncertainty Propagation and Sensitivity Analysis

Lamberto Dell'Elce* and Gaëtan Kerschen†
University of Liège, 4000 Liège, Belgium

DOI: 10.2514/1.G000149

This paper is devoted to the probabilistic uncertainty quantification of orbital lifetime estimation of low-altitude satellites. Specifically, given a detailed characterization of the dominant sources of uncertainty, we map this input into a probabilistic characterization of the orbital lifetime through orbital propagation. Standard Monte Carlo propagation is first considered. The concept of drag correction is then introduced to facilitate the use of polynomial chaos expansions and to make uncertainty propagation computationally effective. Finally, the obtained probabilistic model is exploited to carry out stochastic sensitivity analyses, which in turn allow gaining insight into the impact uncertainties have on orbital lifetime. The proposed developments are illustrated using one CubeSat of the QB50 constellation.

Nomenclature

A	=	surface, m^2
A_p	=	geomagnetic activity index, deg
A_v	=	Avogadro number, mol^{-1}
a_α	=	αth coefficient of the surrogate model
C_d	=	drag coefficient
$\mathcal{E}$	=	objective function in the polynomial chaos expansion method
e	=	orbital eccentricity
$\mathcal{F}$	=	cumulative distribution function of a random variable
$F_{10.7}$	=	daily solar radio flux, solar flux units
$\bar{F}_{10.7}$	=	81-day-averaged solar radio flux, solar flux units
f, g	=	generic functions
h	=	spacecraft altitude from the equatorial radius, m
h_{geo}	=	local altitude from reference ellipsoid, m
$\mathcal{I}$	=	support of a random variable
i	=	orbital inclination, deg
Lat	=	latitude of the spacecraft, deg
Lon	=	longitude of the spacecraft, deg
M	=	dimension of the random vector $\boldsymbol{X}$
m	=	mass of the spacecraft, kg
N	=	number of samples
n_j	=	number density of the gas species j, m^{-3}
p	=	probability density function of a random variable
$\mathbf{r}$	=	position in the Earth-centered inertial frame, m
T	=	local atmospheric temperature, K
T_w	=	wall temperature, K
t	=	time, s
$\mathbf{v}_{ej}$	=	ejection velocity, m/s
v_{ej}	=	norm of the ejection velocity, m/s
$\mathbf{v}_{\text{TAS}}$	=	true airspeed of the spacecraft, m/s
X	=	generic stochastic variable
$\boldsymbol{X}$	=	generic stochastic vector
$\boldsymbol{x}$	=	generic deterministic vector
Y	=	variable of interest, lifetime, day
y	=	single realization of the variable of interest
z	=	generic parameter
α	=	multi-index
δ	=	angle of attack, deg
ϵ	=	roll angle, deg
η	=	model error of a numerical model
Θ	=	spherical angle (azimuth) of the ejection velocity, deg
λ	=	product between drag coefficient and total density, kg/m^3
μ	=	mean value of a random variable
ρ	=	atmospheric density, kg/m^3
Σ	=	drag correction factor
σ	=	standard deviation of a random variable
χ	=	spherical angle (declination) of the ejection velocity, deg
Ψ_α	=	multivariate polynomial with order defined by α
ψ_j	=	univariate polynomial of order j
Ω	=	right ascension of the ascending node, deg

Subscripts

dim	=	dimensional
j, k	=	generic indexes
l	=	relative to the initial conditions before ejection and launcher accuracy
n_j	=	relative to the jth gas species
ref	=	reference condition
T	=	relative to the local atmospheric temperature
$\boldsymbol{X}$	=	relative to the vector $\boldsymbol{X}$
Y	=	relative to the variable of interest
0	=	relative to initial conditions

Superscript

nom	=	nominal condition

I. Introduction

Satellite orbit propagation is a problem for which uncertainty plays a central role [1,2]. Still, uncertainty quantification and propagation is a relatively recent research topic in the astrodynamics community. Park and Scheeres [3] derived fundamental results on the Fokker–Planck equations. Specifically, they proved the integral invariance of the probability density function for diffusionless systems. By exploiting this property and by expressing the analytical solution of a nominal nonlinear trajectory with a Taylor expansion, they developed an analytical representation of the uncertainty propagation of normally distributed initial states. Nonlinear propagation resulted in a progressive distortion of the distribution of the

Received 12 July 2013; revision received 10 June 2014; accepted for publication 19 July 2014; published online 20 October 2014.

*Ph.D. Student, Space Structures and Systems Laboratory, Aerospace and Mechanical Engineering Department, Chemin des Chevreuils 1. Student Member AIAA.

†Professor, Space Structures and Systems Laboratory, Aerospace and Mechanical Engineering Department, Chemin des Chevreuils 1.

propagated states, which became nonnormal. By exploiting adaptive Gaussian mixture models, Giza et al. [4] achieved a tractable expression of the solution of the Fokker–Planck equation, which enabled efficient propagation of uncertainties. In the same work, a simplified drag model was introduced in the dynamic system. Analytical propagation of uncertainties in the two-body problem was then achieved by Fujimoto et al. [5].

The simple numerical implementation, the very relaxed hypotheses, and, more fundamentally, the independence of the convergence rate with respect to problem dimension make the Monte Carlo (MC) simulation method one of the most popular approaches for uncertainty propagation [6]. If the computational cost of a single evaluation of the model is high or if a fine convergence of the statistics of the variable of interest has to be achieved, a well-converged MC propagation may become prohibitive. It is precisely the case for orbital lifetime, which is characterized by a nonlinear long-period propagation and by a large standard deviation. Smart MC sampling techniques (e.g., Markov-chain Monte Carlo) and stochastic expansion techniques overcome this issue by drastically reducing the number of necessary samples. This is why Jones et al. [7–9] introduced the polynomial chaos expansion (PCE) method [10] in astrodynamics.

The main focus of the present paper and of its companion [11] is the prediction of the uncertainties in the orbital lifetime of satellites at low altitudes. Because of the stochastic nature of the atmosphere and the complexity of drag modeling [12], such a prediction should be embedded in an appropriate probabilistic framework. This is why a computationally efficient and nonintrusive propagation of the uncertainties affecting orbital lifetime calculations is proposed herein. Standard MC and PCE methods are both considered, and their performance is compared. Because the cost of PCE (and of stochastic collocation techniques in general) is intimately related to the dimension of the problem (i.e., it grows exponentially with the number of evaluations when considering fully tensorized expansions), a novel methodology for condensing the uncertain variables inherent to the drag force into a single random variable, termed the drag correction factor, is developed. Once a probabilistic description of orbital lifetime is achieved, information about the propagation mechanisms and the relative importance of the different uncertainty sources can be carried out using sensitivity analysis. Global sensitivity analysis is used for attributing percentage of the standard deviation of the lifetime to its inputs. Local sensitivity analysis is also considered for assisting decision and managing uncertainty during the mission design phase.

To illustrate the proposed methodology, the standard two-unit CubeSat of the QB50 constellation [13], proposed by the von Kármán Institute for Fluid Dynamics in Belgium, is considered. This case study is particularly relevant for two reasons. First, the objective of the constellation is to study in situ the spatial and temporal variations in the lower thermosphere. The initial circular orbit will have an altitude of 320 km where atmospheric drag, one of the dominant uncertainty sources in astrodynamics, is significant. Second, it is a real-life mission that should be launched in mid-2015; hence, the results described here can be useful not only to the astrodynamics community but also to the CubeSat developers. The simulation parameters are summarized in Table 1. We point out that some findings of the paper are intimately related to this specific case study. Specifically, the QB50 orbit is near circular, which makes uncertainty in the eccentricity insignificant. Another important assumption concerns the order of magnitude of the lifetime (or of the remaining lifetime if the satellite is already in orbit), which is assumed to be on the order of a fraction of the 11 year solar cycle. This latter assumption is more intrinsic to the proposed methodology because of the particular characterization of the space weather that was carried out in the companion paper [11].

The paper is organized as follows. Section II briefly reviews the outcome of the characterization of the uncertainty sources carried out in [11]. Section III computes the probability density function (PDF) of the orbital lifetime using standard MC propagation and presents interesting findings that can be drawn from this PDF. A reduction of the number of uncertainty sources is then performed in Sec. IV through a preliminary sensitivity analysis and the concept of drag correction factor. This reduction paves the way for an efficient exploitation of PCE in Sec. V. Section VI is devoted to a more thorough sensitivity analysis, and Sec. VII describes a second test case involving the NanoSail-D2 spacecraft. Finally, conclusions of this study are drawn in Sec. VIII.

Table 1 Nominal parameters for the simulations

Variable	Value
Initial conditions	
Initial altitude	320 km
Eccentricity	0
Orbital inclination	79 deg
Launch date	April 2015
Spacecraft properties	
Mass	2 kg
Size	$0.2 \times 0.1 \times 0.1$ m

II. Review of Uncertainty Source Characterization

A prerequisite for uncertainty propagation is that the relevant sources of uncertainty have been identified and properly characterized, that is, their PDF has been determined (e.g., using parametric or nonparametric statistical methods). The two main sources of uncertainties that were found to be important in [11] are the initial states and the atmospheric drag. Table 2 lists the 15 uncertain variables that were investigated during the uncertainty characterization process. The corresponding distributions together with the identified parameters are also given in this table.

The uncertainties in the initial conditions are due to launch date t_0, launcher injection accuracy, a partial knowledge of the orbital parameters, and the ejection velocity $\mathbf{v}_{ej}$. A preliminary combination

Table 2 Summary of the uncertainty sources of the problem

Variable	Symbol	Units	Stochastic modeling
Launch date	t_0	day	Uniform in [4 Jan. 2015, 4 Jan. 2015]
Initial altitude (before injection)	$h_{0,l}$	km	Truncated Gaussian $[0, +\infty)$, 320 km mean, 2.5 km standard
Initial inclination (before injection)	$i_{0,l}$	deg	Gaussian with 89 deg mean and 0.03 deg standard
Initial eccentricity (before injection)	$e_{0,l}$	— —	Truncated Gaussian $[0, +\infty)$, 0 mean, 3.5×10^{-4} standard
Initial RAAN (before injection)	$\Omega_{0,l}$	deg	Uniform in [0, 360] deg
Ejection velocity (norm)	v_{ej}	m/s	Uniform in [1, 1.5] ms^{-1}
Ejection velocity (azimuth)	Θ	deg	Uniform in [0, 360] deg
Ejection velocity (elevation)	χ	deg	Cosine distribution in [−90, 90] deg
Daily solar activity	$F_{10.7}$	sfu	Histogram distribution correlated with $\bar{F}_{10.7}$ and A_P
18 day averaged solar activity	$\bar{F}_{10.7}$	sfu	Histogram distribution correlated with $F_{10.7}$ and A_P
Geomagnetic index	A_p	— —	Histogram distribution correlated with $F_{10.7}$ and $\bar{F}_{10.7}$
Model error of the jth number density	η_{n_j}	— —	Gaussian distribution
Model error of the temperature	η_T	K	Truncated Gaussian, temperature dependent
Angle of attack	δ	deg	Gaussian with 0 deg mean and 5/3 deg standard
Roll angle	ϵ	deg	Uniform in [0, 360] deg

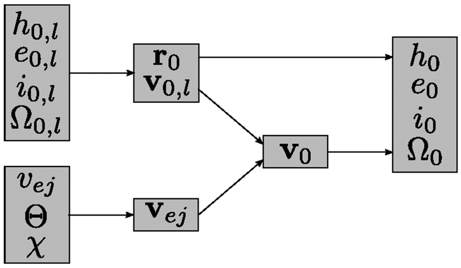

Fig. 1 Precombination of the uncertainties in the initial states.

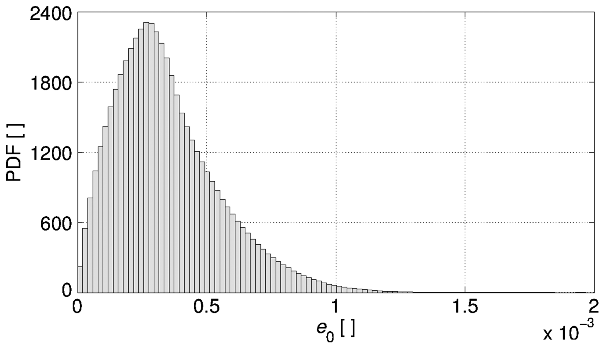

Fig. 2 PDF of the initial eccentricity after injection.

of the uncertainties in the Keplerian parameters is achieved by means of MC propagation following the scheme in Fig. 1. Cartesian position $\mathbf{r}_0$ and velocity $\mathbf{v}_l$ before orbital injection are generated according to the distributions of the altitude $h_{0,l}$, eccentricity $e_{0,l}$, inclination $i_{0,l}$, and right ascension of the ascending node (RAAN) $\Omega_{0,l}$. The final velocity $\mathbf{v}_0$ is calculated by adding the ejection velocity generated with the distributions of the norm of the ejection velocity V and of the spherical angles χ and Θ. Eventually, the initial Cartesian states after ejection, $\mathbf{r}_0$ and $\mathbf{v}_0 = \mathbf{v}_l + \mathbf{v}_{ej}$, are used to compute the corresponding initial orbital parameters h_0, e_0, i_0, and Ω_0. The results of this propagation are a slightly wider distribution for the initial altitude (which still remains Gaussian) and a distortion of the distribution of the eccentricity, as illustrated in Fig. 2, whereas the distributions of the other variables remain unchanged. As explained in [11], the initial true anomaly and argument of perigee were removed from the uncertainty sources.

The uncertainty in the drag force takes its origin from the inherent variability of atmospheric conditions. This variability is due both to stochastic processes in nature (e.g., thermospheric winds and space weather) and to the unmodeled dynamics of the atmosphere (i.e., model driven uncertainty), which is a function of the level of accuracy of the mathematical implementation of the atmosphere and which reflects the evidence that in situ measurements of atmospheric properties do not match the estimations of the models. In this study, we consider the NRLMSISE-00 atmospheric model, whose correlation with space weather is achieved through the daily solar radio flux $F_{10.7}$, 81-day-averaged solar radio flux $\bar{F}_{10.7}$, and geomagnetic activity A_p indices. Other atmospheric models generally require the characterization of different proxies. Model uncertainty is accounted for herein by correcting the outputs of NRLMSISE-00 (i.e., number densities of gas species and temperature) with the random variables η_{n_j} and η_T, respectively. These stochastic variables are characterized according to the bias and standard deviations between the NRLMSISE-00 and in situ observations provided by Picone et al. in [14].

Concerning the characterization of the space weather proxies, different approaches were proposed in the literature to address this important problem [15–17]. Considering them as stochastic processes complicates the uncertainty propagation because the problem belongs to the family of stochastic differential equations [18]. As an alternative for use in orbital lifetime estimation, Fraysse et al. introduced the concept of *constant equivalent solar activity* [19]. The idea is to consider a constant solar flux and geomagnetic index throughout the propagation. If the satellite has a 25 year lifetime for the chosen constant equivalent solar activity, then its lifetime for possible future solar activities will also be 25 years with a probability of 50%. This technique is particularly appropriate for very long propagations on the order of one or several solar cycles. In the companion paper [11], we proposed another approach to the problem. It was also based upon the idea of using an effective solar activity, but it was only suitable for propagations on the order of a fraction of the solar cycle. Instead of a deterministic effective solar activity, we considered a random effective solar activity. The main underlying assumption was that neglecting variations of the space weather proxies with respect to their averaged value in time does not yield drastic variations of the orbital lifetime. To verify this conjecture, we performed two sets of simulations where the solar activity is modeled by means of 1) time series and 2) its temporal average. Then, we compared the resulting orbital lifetime in the two cases, which, for the sake of clarity, we refer to as "true" and "approximated" lifetime, respectively. Specifically, we exploited the stochastic process proposed by Woodburn and Lynch [20] to generate several realizations of the solar activity, and we computed statistics of the difference between the realizations of the true and the approximated lifetime. Finally, we compared this result with the difference between the nominal and the realizations of the true lifetime. The nominal (deterministic) lifetime was computed with the trend of the solar activity according to the long-term Schatten's predictions.[‡] The standard deviation of this difference was one order of magnitude larger than the one of the error between true and approximated lifetime, as illustrated in Fig. 3a. Hence, considering the mean value of each realization of the space weather proxies instead of their complete time history does not introduce significant error compared with the variability of the lifetime. For this reason, $F_{10.7}$, $\bar{F}_{10.7}$, and A_p can be considered in the context of this study as three different random variables that are constant during a single simulation. The characterization of the PDFs of the proxies was finally achieved by identifying a mission window in the dimensionless solar cycle and by exploiting historical data of the same dimensionless window of the past cycles to generate the distributions, as illustrated in Fig. 3b. We emphasize that the proposed characterization and handling of the space weather proxies is a conservative assumption, because it leads to an overestimation of the variance of the variable of interest (VOI). In fact, if the selected data set of historical data includes singular events like the Halloween storms of 2003, it means that the corresponding values of the proxies are part of the event space, though they may only occur with an extremely modest probability. On the contrary, modeling solar activity with a stochastic process cannot lead to realizations with a mean value that is as large as the peaks of these singular events. Nonetheless, this is also why the proposed methodology is limited to the case of orbital lifetimes (or remaining lifetime if the satellite is already in orbit) on the order of a fraction of the solar cycle, otherwise the overestimation of the uncertainty in the VOI would be excessive.

Another uncertainty source in the estimation of the drag is the attitude of the satellite, which in this study is modeled with the angle δ between the spacecraft's long axis and the velocity and the roll angle ϵ (see Fig. 4).

In summary, Fig. 5 shows the precombination step together with the 12 uncertain sources that will be propagated in the next section.

III. Uncertainty Propagation via Monte Carlo Sampling

The mapping $y = g(\boldsymbol{x})$ is considered for which the stochastic M-dimensional input vector $\boldsymbol{x}$ and the (scalar) VOI y are defined on the supports $\mathcal{I}_X$ and $\mathcal{I}_Y$, respectively. MC propagation is a means of quantifying uncertainty in the VOI by mapping uncertainties in the inputs through the model $g(\cdot)$. The generation of a set of N realizations $\boldsymbol{x}_1, \boldsymbol{x}_2, \ldots, \boldsymbol{x}_N$ of the stochastic vector $\boldsymbol{X}$ according to the

[‡]This nominal trend is the deterministic component of the time series generated by Woodburn and Lynch [20].

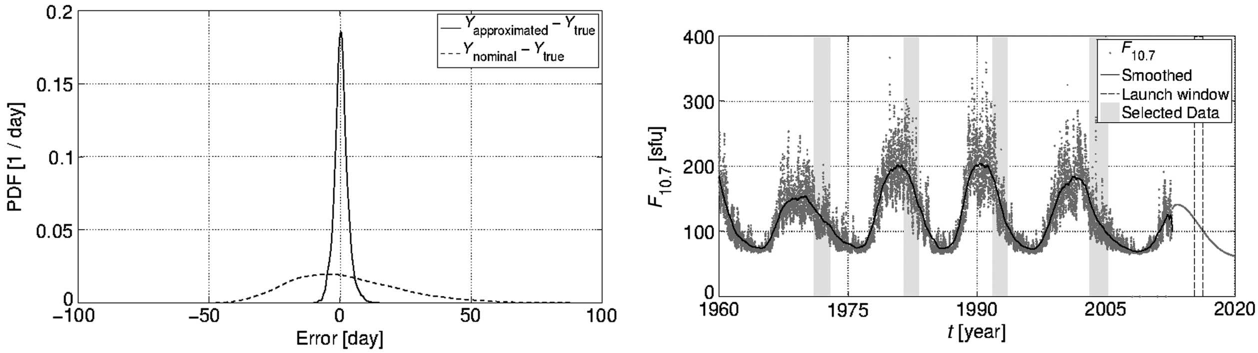

a) PDF of the error between true and approximated orbital lifetime (solid curve), and the PDF of the error between true and nominal lifetime (dashed curve)

b) Selected data set of historical data for QB50

Fig. 3 Characterization of the space weather proxies and validation of the use of the effective solar activity.

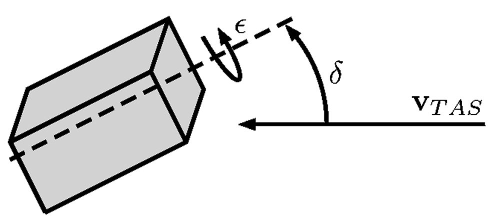

Fig. 4 Notation of the attitude angles; v_{TAS} is the relative incoming airspeed.

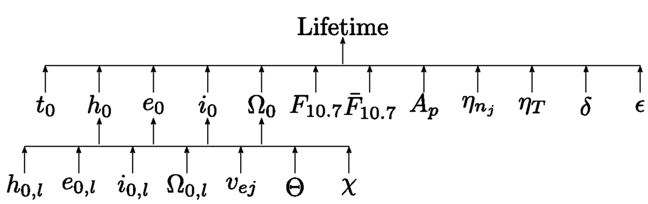

Fig. 5 Schematic representation of the uncertainty propagation process.

joint PDF of its elements is the first step of the MC propagation. Because most of the existing random number generators can only provide with uniformly or normally distributed independent samples, the realization of correlated samples with arbitrary marginal distributions can be carried out by means of a Rosenblatt transformation. In this way, the joint PDF is transformed into a set of uncorrelated standard Gaussian distributions $\mathbf{Z}$, from which MC samples can be directly generated [21]:

$$\left.\begin{matrix} Z_1 \\ \vdots \\ Z_M \end{matrix}\right\} \overset{\text{chol}(C)}{\rightarrow} \left\{\begin{matrix} \Xi_1 & \overset{c_N(\xi_1)}{\rightarrow} & U_1 & \overset{\mathcal{F}^{-1}_{X_1}(u_1)}{\rightarrow} & X_1 \\ \vdots & & & & \\ \Xi_M & \overset{c_N(\xi_M)}{\rightarrow} & U_M & \overset{\mathcal{F}^{-1}_{X_M}(u_M)}{\rightarrow} & X_M \end{matrix}\right. \tag{1}$$

where C_N is the cumulative distribution of the standard Gaussian random variable; $\Xi_1, \ldots, \Xi_M, U, \ldots, U_M$, and $\mathcal{F}_{X_1}, \ldots, \mathcal{F}_{X_M}$ are a set of M-correlated standard Gaussian random variables, a set of M-correlated uniform random variables with support [0, 1], and the cumulative distribution functions of the marginal distributions of $\boldsymbol{X}$, respectively; chol(C) is the Cholesky decomposition [22] of the correlation matrix of $\Xi_1, \ldots, \Xi_M$, and it relates them to the corresponding set of uncorrelated standard Gaussian distribution [i.e., $\boldsymbol{\Xi} = \text{chol}(C)^T \boldsymbol{X}$]. For continuous random variables, the mapping from $\boldsymbol{X}$ to $\boldsymbol{Z}$ is bijective.

The direct evaluation of the mapping for each generated sample leads to N samples of the VOI from which statistics can be computed. Specifically, the second-order descriptors are given by

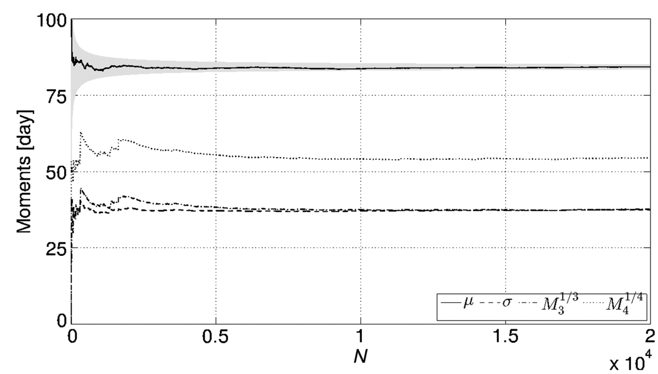

Fig. 6 Convergence of the statistical descriptors of orbital lifetime (MC propagation). The envelope of the shaded area is determined using the bounds $\mu_Y \pm 3(\sigma_Y/\sqrt{N})$.

$$\mu_Y^{(N)} = \frac{1}{N} \sum_{j=1}^{N} y_j \tag{2}$$

$$\sigma_Y^{(N)} = \sqrt{\frac{1}{N-1} \sum_{j=1}^{N} (y_j - \mu_Y^{(N)})^2} \tag{3}$$

The convergence and rate of convergence of MC propagation are ensured by the law of large numbers and the central limit theorem under limited assumptions. This and more general results on the convergence of MC analysis are available in [23,24]. If the mean value μ_Y of the VOI exists, the law of large numbers states that the sample mean $\mu_Y^{(N)}$ converges almost surely to μ_Y as N increases. If the standard deviation σ_Y of the VOI exists and if Lindeberg's condition is satisfied, the central limit theorem states that the error $\mu_Y^{(N)} - \mu_Y$ is a normally distributed random variable with zero mean and standard deviation $\sigma_Y/\sqrt{N}$. We stress that μ_Y and σ_Y are not a property of the mapping $g(\boldsymbol{x})$, because they are intimately related to the characterization of the uncertainty sources, and they cannot account for uncertainty sources that are not modeled.

The MC algorithm was used to compute the orbital lifetime of one nanosatellite of the QB50 constellation considering the 12 uncertainty sources in Fig. 5. Figure 6 shows that 20,000 evaluations were necessary for achieving the convergence of the mean value within ± 1 day with a confidence level of 3σ. The convergence of the higher-order statistical descriptors is also depicted in this figure. Because a single orbital propagation lasts 10 min on average, the complete propagation was run on a computer cluster thanks to the parallelization capabilities of the DAKOTA software [25]; it resulted in an accumulated computational burden of 139 days.

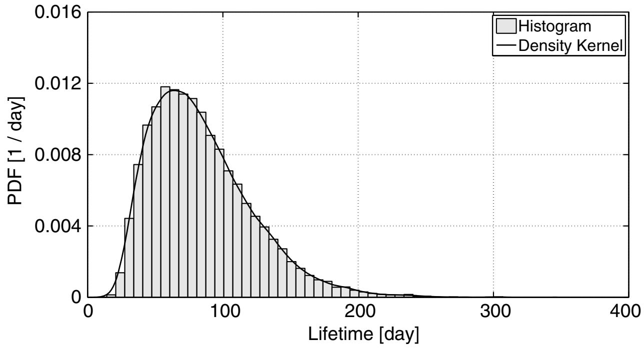

Fig. 7 Histogram and kernel density estimations of the PDF of the orbital lifetime (MC propagation).

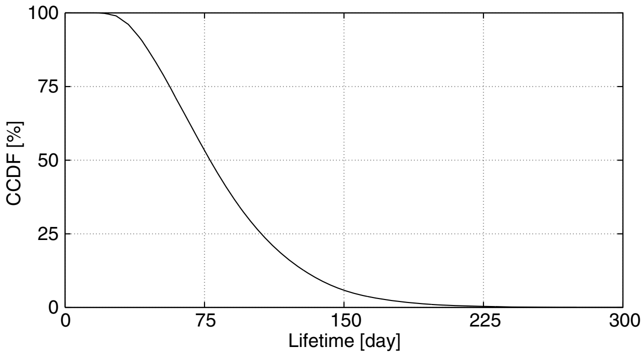

Fig. 8 Complementary cumulative distribution function of orbital lifetime (MC propagation).

Histogram distribution and Gaussian kernel density estimation [26,27] were then implemented to derive a nonparametric representation of the PDF of orbital lifetime. They are presented in Fig. 7. Very useful information can be inferred from Figs. 6 and 7:

1) The mean orbital lifetime is 84.3 days, which is somewhat smaller than the desired lifetime of three months. We note that the mean does not correspond to the peak of the distribution because the PDF is characterized by a nonnegligible (positive) skewness.

2) The standard deviation amounts to 37.5 days, which results in standard deviation to mean ratio of about 0.45. This reflects a substantial, but expected, variability of orbital lifetime that invalidates any deterministic estimation of this quantity.

3) The lifetime can be as short as 14 days and as long as 347 days depending on the considered input sample. The minimum and maximum lifetime correspond to an initial altitude h of 316 and 322 km and a daily radio flux $F_{10.7}$ of 72 and 273 solar flux units (sfu), respectively.

Figure 8 depicts the complementary cumulative distribution function (CCDF) of orbital lifetime. It shows that there is a 6% probability to have a lifetime of 150 days or more. Conversely, there is a nonnegligible probability (i.e., 18%) to have a lifetime shorter than 50 days, which may compromise the success of the mission. Further analysis of these results will be performed in Sec. VI using stochastic sensitivity analysis.

IV. Reduction of the Uncertainty Sources

Although appealing by its simple numerical implementation and by the independence of the convergence rate with respect to the number of uncertainty sources, the MC method has a rate of convergence of order $N^{-1/2}$, which may demand computational resources that are not within reach. Stochastic expansion techniques, such as PCE described in Sec. V, have the capability to drastically reduce the number of necessary samples. However, one limitation of PCE is that the number of quadrature points necessary for the evaluation of the surrogate model depends both on the dimension of the stochastic domain and on the order of the expansion, as detailed in Sec. V.A. For this reason, the number of input random variables with an associated high polynomial order should not be too large. Considering the 12 uncertainty sources of this study together with their nonlinear relations with the VOI, uncertainty propagation cannot be addressed as such using PCE. For this reason, the possibility to obtain a reduced set of uncertainty sources is investigated in this section.

A. Uncertainty in the Initial Orbital Parameters

A preliminary sensitivity analysis for the initial orbital parameters is first achieved to see whether one or several of these variables can be removed from the set of input variables. It consists of measuring the difference between the lifetime computed for the nominal conditions and the lifetime computed by applying a perturbation of one standard deviation to each input sequentially. Because the initial RAAN and launch date are uniformly distributed, the sensitivity analysis is performed by keeping these two variables as parameters. To this end, a grid of 9×11 uniform intervals is considered for the initial RAAN and date, respectively. Table 3 lists the minimum and maximum relative variations of the lifetime on the grid considering perturbations of the initial altitude, eccentricity, and inclination. The variations due to the drag correction factor, which is defined in the next section, are also shown for the purpose of comparison. This table shows that the initial inclination and eccentricity are responsible for tiny variations of the orbital lifetime; they can be safely neglected in our analysis. We note that this finding is related to the QB50 case study. In addition, the argument of perigee could also be a relevant variable for eccentric orbits. On the contrary, given the high cost of out-of-plane maneuvers, neglecting uncertainty in the inclination is a more general result. For the sake of completeness, we also note that, for long-term propagations, uncertainty in the initial true anomaly is irrelevant if initial states are provided in terms of mean elements.

In conclusion, targeting a reduction of the dimension of the problem, a preliminary sensitivity analysis is encouraged. Case-dependent results should be expected from this analysis.

B. Uncertainty in the Drag Force

1. *Drag Correction Factor*

We now propose to reduce all the uncertainties affecting the drag force into a single stochastic variable through a precombination process analogous to the one illustrated in Fig. 1. This method is developed ad hoc for the problem of uncertainty quantification of lifetime in low Earth orbit (LEO), but the methodology could be extended to other problems in astrodynamics.

The drag force is calculated through the NRLMSISE-00 atmospheric model [14] in our orbital propagations. This model gives an estimation of the number densities of the different gas species n_j^{model} and of the local atmospheric temperature T^{model} for specified longitude (Lon), latitude (Lat), Julian date (JD), altitude from ellipsoid h_{geo}, solar $F_{10.7}$, $\bar{F}_{10.7}$, and geomagnetic activity A_p indices:

$$[n_j^{\text{model}}, T^{\text{model}}] = \text{NRLMSISE} - 00\,(\text{Lon}, \text{Lat}, \text{JD}, h_{\text{geo}}, F_{10.7}, \bar{F}_{10.7}, A_p) \quad (4)$$

To account for the inherent uncertainty of atmospheric conditions, corrected atmospheric properties were defined in [11] using random variables η_{n_j} and η_T:

Table 3 Preliminary sensitivity analysis: minimum/maximum variations of the lifetime for 1σ perturbation of the input

	Minimum variation, %	Maximum variation, %
Initial altitude	5.3	6.4
Initial eccentricity	0.01	0.11
Initial inclination	2.4×10^{-4}	0.01
Drag correction factor	28.4	33.3

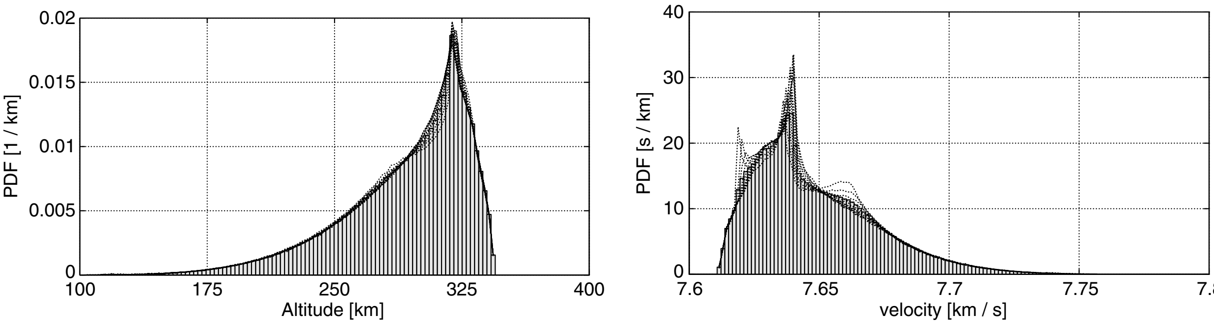

a) Altitude

b) Velocity

Fig. 9 PDF of the altitude h_{geo} and of the velocity v_{TAS}. Each dotted line shows the distribution obtained with the samples of a single orbital propagation. Histogram are evaluated with the samples of all the propagations.

$$n_j = n_j^{\text{model}} \exp(\eta_{n_j}) \tag{5}$$

$$T = T^{\text{model}} + \eta_T \tag{6}$$

The resulting atmospheric density is

$$\rho = \frac{1}{Av} \sum_j n_j m_j$$

where Av is the Avogadro number and m_j is the molar mass of the jth species. The drag coefficient is computed using the updated Sentman model [28–30]:

$$C_d = C_d\,(\text{Lon}, \text{Lat}, \text{JD}, h_{\text{geo}}, v_{\text{TAS}}, T_w, \eta_T, \eta_{n_j}, \delta, \epsilon) \tag{7}$$

where v_{TAS}, T_w, δ, and ϵ represent the bulk velocity of the air with respect to the satellite, the wall temperature, and the angles characterizing satellite attitude, respectively. The dependency on the wall temperature is omitted in the remainder of this paper because of the low sensitivity of the drag coefficient with respect to this variable [11,12].

The variable λ is introduced as the product between the drag coefficient and the atmospheric density:

$$\begin{aligned}\lambda &= C_d \rho \\ &= \lambda\,(\text{Lon}, \text{Lat}, \text{JD}, h_{\text{geo}}, v_{\text{TAS}}; F_{10.7}, \bar{F}_{10.7}, A_p, \eta_T, \eta_{n_j}, \delta, \epsilon)\end{aligned} \tag{8}$$

The inputs before the semicolon are computed as a function of the current states and time during the propagation, whereas the other inputs are stochastic variables that were characterized in [11]. A nominal value is now defined for each stochastic variable. Specifically, $\eta_T^{\text{nom}} = \eta_{n_j}^{\text{nom}} = 0$, whereas the nominal value of the other parameters is selected as the expected value of their distribution. The *drag correction factor* Σ is defined as

$$\begin{aligned}\Sigma &= \frac{\lambda(\text{Lon},\text{Lat},\text{JD},h_{\text{geo}},v_{\text{TAS}};F_{10.7},\bar{F}_{10.7},A_p,\eta_T,\eta_{n_j},\delta,\epsilon)}{\lambda(\text{Lon},\text{Lat},\text{JD},h_{\text{geo}},v_{\text{TAS}};F_{10.7}^{\text{nom}},\bar{F}_{10.7}^{\text{nom}},A_p^{\text{nom}},\eta_T^{\text{nom}},\eta_{n_j}^{\text{nom}},\delta^{\text{nom}},\epsilon^{\text{nom}})} \\ &= \frac{\lambda(\text{Lon},\text{Lat},\text{JD},h_{\text{geo}},v_{\text{TAS}};F_{10.7},\bar{F}_{10.7},A_p,\eta_T,\eta_{n_j},\delta,\epsilon)}{\lambda^{\text{nom}}(\text{Lon},\text{Lat},\text{JD},h_{\text{geo}},v_{\text{TAS}})}\end{aligned} \tag{9}$$

so that, without any loss of generality, the drag force is given by

$$\boldsymbol{F}_d = -\frac{1}{2}\frac{A_{\text{ref}} C_d}{m} \rho v_{\text{TAS}} \boldsymbol{V}_{\text{TAS}} = -\frac{1}{2}\frac{A_{\text{ref}}}{m} \Sigma \lambda^{\text{nom}} v_{\text{TAS}} \boldsymbol{V}_{\text{TAS}} \tag{10}$$

where A_{ref} and m are a reference surface and the mass of the spacecraft, respectively. Equation (10) is just a mathematical manipulation because the drag correction factor is formally defined as a function of all the inputs of drag force; the two expressions of the drag force in Eq. (10) are equivalent. In the following, we introduce assumptions aimed at approximating the drag correction factor to convert it into a random variable that accommodates all the modeled uncertainty sources in the drag force. The main advantage of this method is that the uncertainties inherent to $F_{10.7}, \bar{F}_{10.7}, A_p, \eta_T, \eta_{n_j}, \delta$, and ϵ can be combined into the only variable Σ, thereby reducing greatly the number of random variables for the subsequent propagation of orbital lifetime using PCE.

Equation (9) shows that the drag correction factor is, in principle, a function of the stochastic inputs of the problem and of Lon, Lat, JD, h, and v_{TAS}, which we refer to as "state-dependent" variables, because they can be deduced from the current states of the satellite and propagation time. Indeed, they generally also depend on the random variables of the problem. For instance, the Julian date is given by $\text{JD} = \text{JD}_0 + t$. A critical assumption we make here is that the correlation between the drag correction factor and the state-dependent variables is negligible, which means that the error in the drag made when considering the nominal conditions of the stochastic variables instead of their current conditions weakly depends on the state-dependent variables. This assumption is not given, and it needs to be validated. Section IV.B.2 discusses its validation.

Provided that this assumption is valid, the idea behind the proposed method is to characterize the drag correction factor as a random variable by temporally modeling the state-dependent variables as random. In this way, the PDF of the drag correction factor can be evaluated through the evaluation of Eq. (9).

The modeling of the state-dependent variables is performed by answering the question: What is the probability to have a certain value of the variable during the mission? Because the orbit of the case study is near circular, latitude and longitude are modeled as uniform random variables with support $\mathcal{I}_{\text{Lat}} = [-i, i]$ where $i = 79$ deg is the reference orbital inclination and $\mathcal{I}_{\text{Lon}} = [-180, 180]$ deg, respectively. Given the one year launch window, the Julian date is modeled as a uniform random variable with support $\mathcal{I}_{\text{JD}} = [1\ \text{Jan.}, 31\ \text{Dec.}]$.[§] To compute the joint distribution of z and v_{TAS}, orbital propagations were carried out for various levels of solar and geomagnetic activities, whereas all the other parameters were set to their nominal value. Altitude and velocity were sampled with a fine time step to generate the distributions of Fig. 9. In particular, each dotted line is a distribution relative to one specific orbital propagation, whereas the histograms are built by considering all the samples of all the simulations. The dotted curves were added to Fig. 9 to show that the percentage of the orbital time spent at a certain altitude is not strongly affected by the duration of the lifetime itself (which in these simulations spans from about 40 to 90 days). Strictly speaking, the satellite falls slowly in quiet periods, but the percentage of its orbital time spent at a certain altitude is similar to the one obtained during an active period. The distributions of the velocity are extremely narrow, so that, even if their shape changes from one propagation to the other (compared with the altitude), it will not yield significant variations of the drag correction factor. An important correlation of −97% relates the two marginal PDFs.

[§]The NRLMSISE-00 model does not take into account long-term trends; specifying the year is therefore irrelevant.

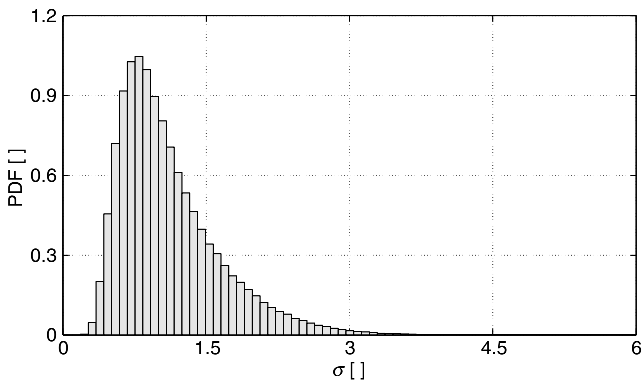

Fig. 10 PDF of the drag correction factor Σ (MC propagation with 10^6 samples).

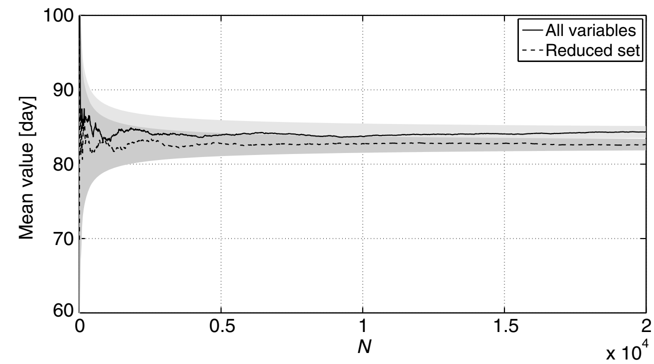

Fig. 11 Convergence of the mean value of the lifetime with the MC propagation. Bounds are given by $\mu_Y \pm 3(\sigma_Y/\sqrt{N})$, where μ_Y, σ_Y, and N are the final mean value, the final standard deviation, and the current number of samples, respectively.

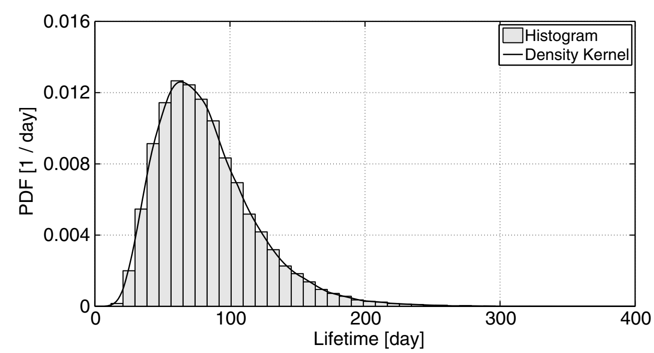

Fig. 12 Histogram and density kernel estimation of the PDF of the lifetime obtained through the MC propagation of the reduced set of uncertainty sources (20,000 samples).

We stress that this characterization of the state-dependent variables is intimately related to our case study. Specifically, the uniform characterization of the latitude does not hold for elliptic orbits. In that case, they should be characterized together with the orbital altitude and velocity by means of numerical evaluation of their distributions through a certain number of supporting orbital propagations. Their correlations should be accounted for as well. We also note that the correlation between longitude and Julian date can be significant for sun-synchronous orbits. Because the considered orbit is not sun-synchronous, the local sidereal time is uniformly distributed between 0000 and 2400.

The PDF of the drag correction factor resulting from the Monte Carlo propagation of 10^6 samples of the different input variables is presented in Fig. 10. The PDF shows that the error due to drag estimation with nominal conditions for the stochastic inputs can be as severe as 200% (i.e., when $\Sigma = 3$). Even if the uncertainty can be reduced as more information about the mission is available (e.g., precise knowledge of attitude dynamics), Sec. IV.B.2 will show that the main contributor to the drag correction factor is the solar activity, whose uncertainty is irreducible.

2. *A Priori and A Posteriori Validation of the Assumption*

The values of two statistical indicators are given in Table 4 to validate the assumption of weak dependency of the formal definition of the drag correction factor [i.e., Eq. (9)], with respect to the state-dependent variables. Spearman's rank correlation measures if the relationship between the drag correction factor and the considered input variable can be described using a monotonic relation. It is defined as Pearson's correlation coefficient, but the values of the variables are replaced with their ranks. The total-effect Sobol index, defined between zero and one, is a measure of the contribution of the uncertainty of the considered input variable in the generation of the uncertainty in the drag correction factor. In other words, it indicates the contribution of an input in the generation of the uncertainty in the VOI. This contribution also accounts for the interaction of the input in analysis with the others. More details on Sobol indices are available in Sec. VI.A.

Table 4 Spearman and Sobol indices of the drag correction factor with respect to all the inputs

Input	Spearman, %	Sobol, %
$F_{10.7}$	75.84	55.92
$\bar{F}_{10.7}$	79.34	62.13
A_p	28.68	7.84
η_{He}	0.57	0.90
η_O	37.90	15.50
η_{N_2}	25.00	7.30
η_{Ar}	−0.04	0.90
η_H	−0.22	0.90
η_N	1.38	0.91
η_T	1.52	0.94
δ	0.33	1.28
ϵ	−0.34	0.91
Lon	0.04	0.96
Lat	0.05	0.78
JD	0.41	1.01
h_{geo}	−3.19	0.92
v_{TAS}	3.14	0.87

Spearman indices show that the five state-dependent inputs are weakly correlated with the drag correction factor, as it was assumed. Conversely, this factor is strongly correlated with a subset of the uncertain parameters, namely, the solar and geomagnetic activity indices, and the model correction factors of total oxygen and molecular nitrogen. Sobol indices confirm these findings. We refer to this validation as a priori, because it automatically comes with the evaluation of the PDF of the drag correction factor. This cannot be considered generally valid, and it needs to be verified for each specific case study.

A posteriori validation of the assumption can also be carried out by comparing the outcome of Monte Carlo propagations for orbital lifetime for both the full and reduced set of uncertain parameters. The results are depicted in Figs. 11 and 12. Table 5 summarizes the error between the two propagations in terms of the first four moments and of the relative entropy, which can be seen as a nonsymmetric measure of the difference between two probability distributions. The absolute error on the mean value is less than two days, which is largely smaller than the standard deviation. Furthermore, the error does not grow radically with the order of the moments with the consequence that the two distributions have a very similar shape (compare with Fig. 7). Overall, the proposed reduction strategy gives results that are in good concordance with those obtained with the full set of uncertain variables; they therefore confirm that the state-dependent variables play a very modest role in the characterization of the drag correction factor.

Table 5 Error between the MC propagation with full and reduced set of uncertainty sources

	Reduced set, day	All variables, day	Error, %
Mean	82.6	84.3	−2.01
Standard deviation	36.6	37.5	−2.40
$\sqrt[3]{\boldsymbol{M}_3}$	39.2	37.7	3.98
$\sqrt[4]{\boldsymbol{M}_4}$	56.9	54.5	4.40
Relative entropy	— —	— —	0.45

V. Efficient Uncertainty Propagation via Polynomial Chaos Expansion

A. Theoretical Background

PCE belongs to the family of stochastic expansion methods [10]. These algorithms generally involve two steps, namely, the construction of a computationally efficient surrogate model of the system and the stochastic propagation through both analytical and numerical evaluation of the surrogate model. Several techniques are available to calculate the coefficients of the expansion. They involve embedded projection, collocation, and nonintrusive projection [31–33]. This latter technique is discussed in this paper.

Consider a set of M uncertain independent variables $\boldsymbol{X} = (X_1, \ldots, X_M)^T$ defined on the support $\mathcal{I}_{\boldsymbol{X}}$ and with joint PDF

$$p_{\boldsymbol{X}}(\boldsymbol{x}) = \prod_{j=1}^{M} p_{X_j}(x_j)$$

The deterministic application $y = g(\boldsymbol{x})$ with $g\colon \mathcal{I}_{\boldsymbol{X}} \to \mathcal{I}_Y$ maps a single sample of $\boldsymbol{X}$ into a sample of the VOI Y, which is the lifetime here. PCE consists in determining a polynomial surrogate model $\hat{g}(\boldsymbol{X})$ such that

$$g(\boldsymbol{x}) \approx \hat{g}(\boldsymbol{x}) = \sum_{\boldsymbol{\alpha}=0}^{\boldsymbol{\alpha}^{\max}} a_\alpha \Psi_\alpha(\boldsymbol{X}) \tag{11}$$

where

1) $\boldsymbol{\alpha} = (\alpha_1, \alpha_2, \ldots, \alpha_M)^T \in \mathbb{N}^M$ is a multi-index vector. The summation on α is such that

$$\sum_{\boldsymbol{\alpha}=0}^{\boldsymbol{\alpha}^{\max}} (\cdot) = \sum_{\alpha_1=0}^{\alpha_1^{\max}} \sum_{\alpha_2=0}^{\alpha_2^{\max}} \ldots \sum_{\alpha_M=0}^{\alpha_M^{\max}} (\cdot) \tag{12}$$

2) $\boldsymbol{\alpha}^{\max} = (\alpha_1^{\max}, \alpha_2^{\max}, \ldots, \alpha_M^{\max})^T \in \mathbb{N}^M$ is a user-supplied vector defining the maximum order of the polynomial model for each component of $\boldsymbol{X}$.

3) $[\Psi_0, \ldots, \Psi_{\boldsymbol{\alpha}^{\max}}]$ is a basis of multivariate polynomials that are orthonormal with respect to the inner product $\langle\cdot,\cdot\rangle_{p_{\boldsymbol{X}}}$, defined as $\langle f, g\rangle_{p_{\boldsymbol{X}}} = \int_{\mathcal{I}_{\boldsymbol{X}}} f(\boldsymbol{x}) g(\boldsymbol{x}) p_{\boldsymbol{X}}(\boldsymbol{x})\, \mathrm{d}\boldsymbol{x}$. The generic term $\Psi_{\boldsymbol{\alpha}}$ is given by

$$\Psi_{\boldsymbol{\alpha}}(\boldsymbol{x}) = \prod_{j=1}^{M} \psi_j^{\alpha_j}(x_j) \tag{13}$$

where $[\psi_j^0, \ldots, \psi_j^{\alpha_j^{\max}}]$ is a basis of univariate polynomials of order $[0, \ldots, \alpha_j^{\max}]$ orthonormal with respect to $\langle\cdot,\cdot\rangle_{p_{X_j}}$ (e.g., Hermite and Legendre polynomials for standard normal and uniform distributions on $[-1, 1]$, respectively).

4) a_α is an M-order tensor of unknown coefficients.

The choice of the coefficients a_α is performed by minimizing the functional

$$\mathcal{E} = \frac{1}{2}\|g - \hat{g}\|_{p_X}^2 \equiv \frac{1}{2}\langle g - \hat{g}, g - \hat{g}\rangle_{p_X} \tag{14}$$

By setting the derivative of $\mathcal{E}$ with respect to a_α to zero and by exploiting the orthonormality of the basis, the optimality conditions write

$$a_\alpha = \langle g, \Psi_{\boldsymbol{\alpha}}\rangle_{p_X}, \qquad \text{for } \boldsymbol{\alpha} = 0, \ldots, \boldsymbol{\alpha}^{\max} \tag{15}$$

Proper Gaussian quadrature rules are generally exploited for an efficient numerical computation of the integrals involved in Eq. (15). A multidimensional grid with $\alpha_j^{\max} + 1$ gauss points in the jth variable is implemented, which results in

$$\prod_{j=1}^{M} (\alpha_j^{\max} + 1)$$

evaluations of the model g.

Statistical properties of the VOI can then be evaluated by numerical evaluation of the surrogate model using, for example, MC propagation. However, second-order descriptors can be directly deduced from the coefficients a_α by taking advantage of the orthonormal properties of the basis

$$\mu_Y = a_0 \tag{16}$$

$$\sigma_Y^2 = \sum_{\boldsymbol{\alpha}=0}^{\boldsymbol{\alpha}^{\max}} a_\alpha^2 - a_0^2 \tag{17}$$

B. Orbital Lifetime Computations

The DAKOTA software [25] is used for computing the PDF of the orbital lifetime through PCE. The reduced set of uncertainty sources Σ, h_0, t_0, and Ω_0 identified in Sec. IV is considered for this purpose; a summary of the reduction process is given in Fig. 13. Histogram, Gaussian, and two uniform distributions are exploited to model their univariate PDFs, respectively. Even though ad hoc univariate-orthogonal polynomial bases can be generated for any distribution, we mapped our variables into standard distributions to take advantage of labeled polynomials. The normal and uniform distributions were then mapped to standard normal distribution and uniform distributions on $[-1, 1]$, respectively. For the histogram distribution, isoprobability transformations [34] toward both standard normal and uniform distribution on $[-1, 1]$ were considered. According to the convergence criteria defined later in this section, the former distribution was found to be more effective and was therefore retained.

We note that mixing different bases in the presence of correlated inputs might yield to a degradation of the convergence rate of the expansion. In this case, mapping all the input into standard Gaussian variables by means of a Rosenblatt transformation can be beneficial.

The choice of the order $\alpha_j^{\max}$ of the polynomials was performed by computing the PCE, $Y_j^{(\alpha_j^{\max})}$ for each scalar component X_j, while setting the other components to their nominal values. The minimum order $\alpha_j^{\max}$, which provides a weighted mean-squared distance (MSD) with respect to the expansion at the previous order smaller than the 1% of the expected value of $Y_j^{(\alpha_j^{\max})}$, is selected. Figures 14–17 present the convergence for the four variables. As desired, the absolute value of the coefficients of the expansion depicted in the top-right diagrams decreases exponentially for high-order polynomials. The selected orders are 4, 2, 9, and 0 for Σ, h_0, t_0, and Ω_0, respectively.¶

Figure 18 shows the response surfaces obtained with the multivariate PCE. The same qualitative behavior for the univariate response curves in Figs. 14–16 is recognized. Overall, PCE requires only 150 evaluations of the model for the determination of the multivariate expansion. This is a significant improvement over the

¶First-order Hermite polynomial should have been retained for the initial RAAN according to the mean-squared distance. However, in view of the small influence of this variable on the VOI, zero-order polynomials can be safely chosen.

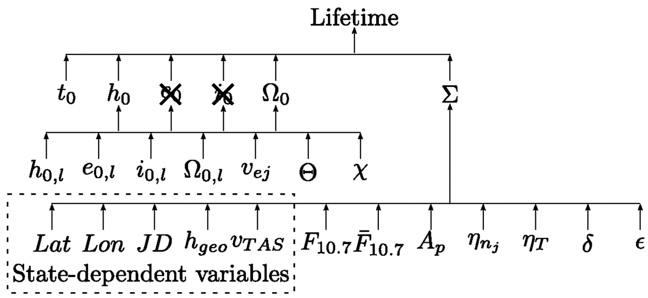

Fig. 13 Schematic representation of the proposed reduction of the uncertainty sources.

MC propagation of Sec. III where 20000 samples were necessary for an adequate convergence of the mean value. In addition, the criterion used for the choice of the order of the PCE expansion is based upon the convergence of the PDF, which is more severe than the convergence of the mean value. Finally, we note that the high-order polynomial characterizing the sensitivity of the VOI with respect to the launch date is due to the nonmonotonic response illustrated in the bottom diagram of Fig. 16. The number of evaluations of the model could be reduced even further if a narrower launch window were identified.

Analytical second-order descriptors are deduced from the PCE coefficients according to Eqs. (16) and (17); they are given in Table 6. In this table, the convergence is also verified by comparing the obtained results both with a refined PCE model where the order of the univariate polynomials is increased by one and with direct MC propagation of the reduced set. All these results indicate that the selected PCE is adequately converged.

Finally, MC propagation using the surrogate model is realized to estimate the PDF of the orbital lifetime. Figure 19 illustrates the density kernel estimation of the PDF obtained for PCE, MC with the reduced set of inputs, and MC with the complete set of inputs. As discussed in Sec. IV.B.2, the assumptions introduced for the characterization of the drag correction as a random variable are responsible for a discrepancy in the mean value of the VOI on the order of two days, which is small compared with the standard deviation of the VOI itself. In addition, with only 150 samples, the 3-sigma confidence bounds in the mean value of the VOI for the MC propagation is as large as 10 days. For these reasons, the compromise between the loss of accuracy due to the reduction of the uncertainty sources and the enhanced computational efficiency given by PCE is satisfactory.

VI. Stochastic Sensitivity Analysis

Uncertainty propagation allows us to obtain a statistical description of the VOI, which is useful for estimating precisely the variability affecting this quantity. The present section is devoted to stochastic sensitivity analysis for gaining insight into the nature of the propagation itself. Such an analysis is relevant for engineering purposes, particularly for decision making and for assessing the efforts needed to reduce uncertainties on the VOI. Both global and local sensitivity analyses are conducted in this study.

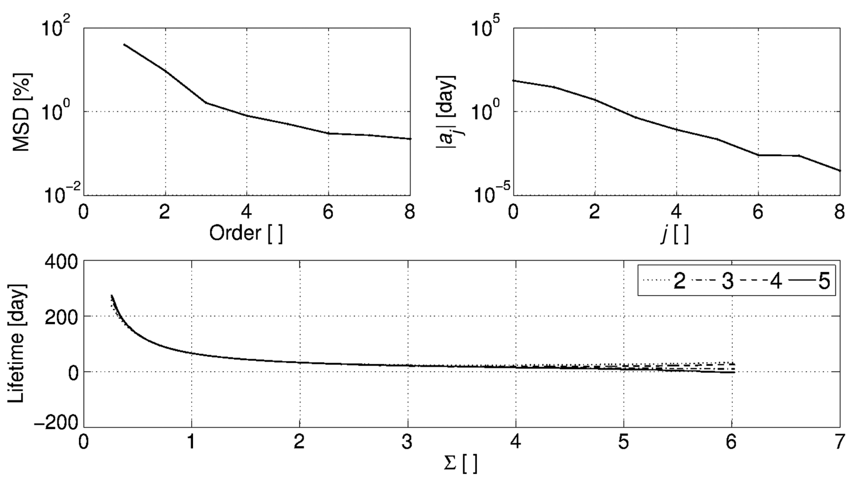

Fig. 14 Drag correction factor: mean-squared distance between consecutive orders (top left), norm of the PCE coefficients (top right), and response curve (bottom).

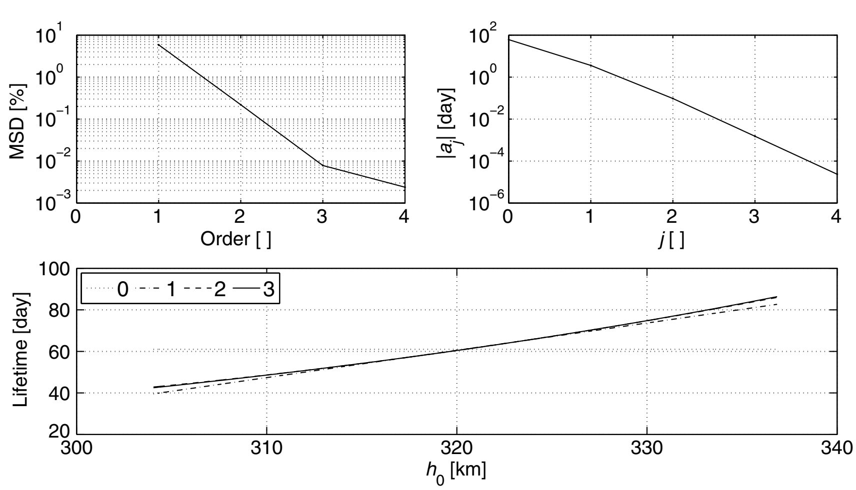

Fig. 15 Initial altitude: mean-squared distance between consecutive orders (top left), norm of the PCE coefficients (top right), and response curve (bottom).

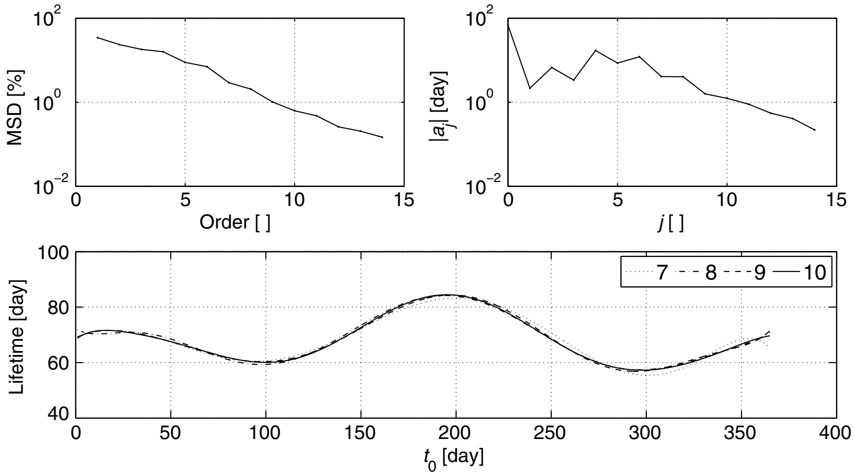

Fig. 16 Launch date: mean-squared distance between consecutive orders (top left), norm of the PCE coefficients (top right), and response curve (bottom).

A. Global Sensitivity Analysis

The objective of global sensitivity analysis is to measure the contribution of each stochastic source in the generation of the uncertainty of the VOI, measured through its variance. The total-effect sensitivity index for the input X_j is the expected value of the variance of the VOI given all the variables but X_j [35,36]

$$\mathbb{E}[\mathrm{Var}(Y|\boldsymbol{X}_{\sim j})] \tag{18}$$

where $\boldsymbol{X}_{\sim j}$ means all the elements of $\boldsymbol{X}$ except the component j. The sensitivity index can be interpreted as the portion of the uncertainty in the VOI that can be attributed to the input X_j and its interactions with other variables. The sensitivity indices are often normalized with the variance of the VOI. These dimensionless coefficients are referred to as *total-effect Sobol indices* in the literature.

The numerical computation consists of the integration of

$$\mathbb{E}[\mathrm{Var}(Y|\boldsymbol{X}_{\sim j})] = \int_{\mathcal{I}_{X_{\sim j}}} \left[\int_{\mathcal{I}_{X_j}} g(\boldsymbol{x})^2 p_{X_j|X_{\sim j}}(x_j|\boldsymbol{x}_{\sim j})\,\mathrm{d}x_j - \left(\int_{\mathcal{I}_{X_j}} g(\boldsymbol{x}) p_{X_j|X_{\sim j}}(x_j|\boldsymbol{x}_{\sim j})\,\mathrm{d}x_j\right)^2\right] p_{X_{\sim j}}(\boldsymbol{x}_{\sim j})\,\mathrm{d}\boldsymbol{x}_{\sim j} \tag{19}$$

where

$$p_{X_j|X_{\sim j}}(x_j|\boldsymbol{X}_{\sim j}) \equiv \frac{p_{\boldsymbol{X}}}{p_{\boldsymbol{X}_{\sim j}}}$$

is the conditional probability of x_j given $\boldsymbol{X}_{\sim j}$. For a set of independent variables,

$$p_{X_{\sim j}}(\boldsymbol{x}_{\sim j}) = \prod_{k=1,k\neq j}^{N} p_{X_k}(x_k) \tag{20}$$

Both deterministic and nondeterministic integration techniques can be implemented for the numerical computation of Eq. (19). The computation of the integrals can be sped up by evaluating a surrogate model if available. In addition, if the surrogate model is built with PCE, Sudret demonstrated that total-effect sensitivity indices can be analytically deduced from the coefficients of the expansion [37]. For an orthonormal basis and an independent set of inputs, it follows that

$$\mathbb{E}[\mathrm{Var}(Y|\boldsymbol{X}_{\sim j})] = \sum_{\boldsymbol{\alpha}\,\mathrm{s.t.}\,\alpha_j>0}^{\boldsymbol{\alpha}^{\max}} a_{\alpha}^2 \tag{21}$$

Table 7 lists the Sobol indices obtained in the case study. The drag correction factor is by far the most important contributor to the uncertainty in the orbital lifetime. This result confirms that a more profound knowledge of drag in rarefied flows and of thermospheric models would be highly beneficial, as heavily stressed in the literature (e.g., [12,20,29,38–40]). However, the stochastic nature of processes such as solar and geomagnetic activities invalidates any deterministic modeling of the drag, as confirmed by the Sobol indices of the drag correction factor in Table 4. This is why stochastic modeling of this problem is particularly relevant and important.

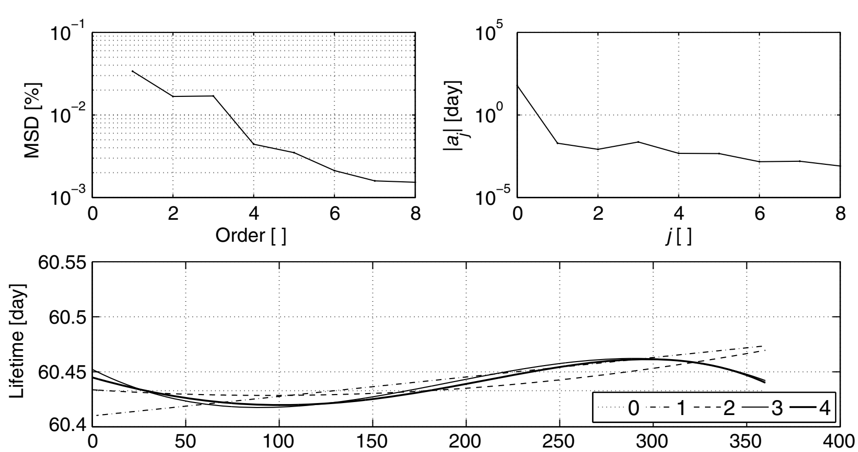

Fig. 17 Initial RAAN: mean-squared distance between consecutive orders (top left), norm of the PCE coefficients (top right), and response curve (bottom).

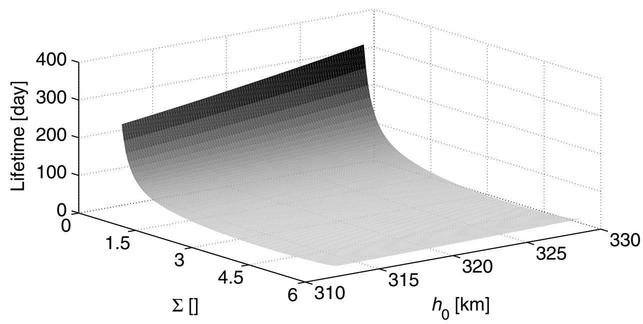

a) Orbital lifetime in function of initial altitude and drag correction factor; t_0 = April the 1st and $\Omega_0 = 0$ deg

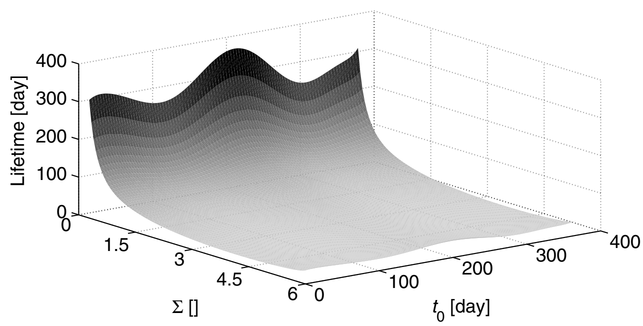

b) Orbital lifetime in function of launch date and drag correction factor; $h_0 = 320$ km and $\Omega_0 = 0$ deg

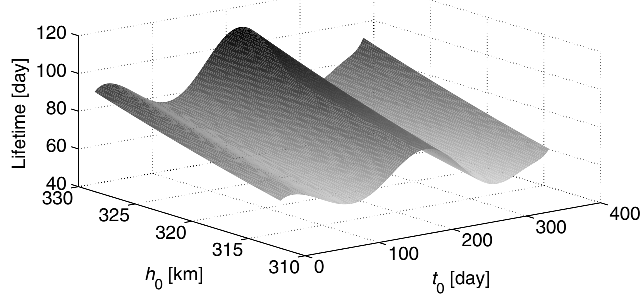

c) Orbital lifetime in function of launch date and initial altitude; $\Sigma = 1$ and $\Omega_0 = 0$ deg

Fig. 18 Response surface obtained with the PCE.

The launch date also has a nonnegligible Sobol index, but this uncertainty will be progressively reduced (and eliminated) in the function of the advancement of mission design. The Sobol index of the initial altitude shows that, unlike drag, improving launcher accuracy would only result in a very modest improvement of the knowledge of orbital lifetime. We note that the impact on uncertainty of initial orbital parameters of an already orbiting object determined with two-line elements (TLE) fitting is potentially much more substantial [41].

Table 6 Convergence of the multivariate PCE[a]

	PCE	PCE refined	MC reduced set	Units
Mean	82.2	82.1 (0.06%)	82.6 (0.52%)	Day
Standard deviation	36.4	36.6 (−0.41%)	36.6 (0.51%)	Day
$\sqrt[3]{\boldsymbol{M}_3}$	39.1	39.3 (−0.60%)	39.2 (0.36%)	Day
$\sqrt[4]{\boldsymbol{M}_4}$	56.7	57.1 (−0.69%)	56.9 (0.32%)	Day
Relative entropy	— —	0.06%	0.06%	— —

[a]Errors with respect to the PCE model are listed in parentheses.

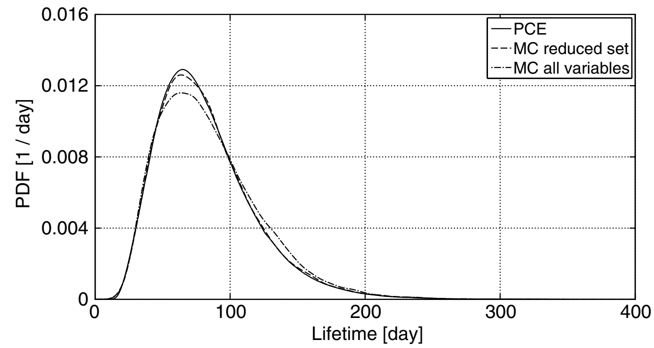

Fig. 19 Comparison of the PDFs obtained with PCE, MC simulation with the reduced set of inputs, and MC simulation with the complete set of inputs.

B. Local Sensitivity Analysis

Derivatives of the VOI with respect to variations of a nominal input are particularly useful in the framework of a deterministic mission analysis and design, because they suggest the "direction" in which the input should be modified to improve nominal performance. Likewise, derivatives of the variance of the VOI with respect to nominal values provide valuable insight into the direction in which the input should be modified to reduce uncertainties. The results of these analyses can be conflicting, and a compromise is then to be achieved. For example, consider a variation in the nominal initial altitude. The derivative of the lifetime with respect to the initial altitude would suggest to increase this parameter to maximize the lifetime. However, because the derivative of the variance is likely to be positive, uncertainty in the lifetime would also increase. It might therefore happen that the expected augmentation in lifetime due to a higher altitude is jeopardized by the higher uncertainty level.

Local sensitivity analysis provides a quantitative means of addressing this compromise between performance and robustness. It is therefore complementary to the global analysis described in the preceding section. It amounts to computing the derivatives of the variance of the VOI, with respect to a generic parameter z related to the characterization of the PDF of the inputs. This analysis is local in the sense that the results are related to a specific point of the input space $\mathcal{I}_X$.

Finite differences are a common way to numerically estimate the derivatives [42]. Pseudoanalytical evaluations are an interesting alternative [43]. To this end, we consider the derivatives of the mean and variance of the VOI with respect to a generic parameter z:

$$\frac{\partial \mu_Y}{\partial z} = \mathbb{E}\left(\frac{\partial Y}{\partial z}\right) \tag{22}$$

$$\frac{\partial \sigma_Y^2}{\partial z} = 2\mathbb{E}\left(Y \frac{\partial Y}{\partial z}\right) - 2\mathbb{E}(Y)\mathbb{E}\left(\frac{\partial Y}{\partial z}\right) \tag{23}$$

where the derivatives of the VOI with respect to the parameter z are derived by means of the chain rule

$$\frac{\partial Y}{\partial z} = \frac{\partial g(\boldsymbol{X})}{\partial z} = \frac{\partial g(\boldsymbol{X}_{\mathrm{dim}}(\boldsymbol{X}; z, \ldots))}{\partial z} = (\nabla_{X_{\mathrm{dim}}} g)^T \frac{\partial \boldsymbol{X}_{\mathrm{dim}}}{\partial z} \tag{24}$$

where $\boldsymbol{X}_{\mathrm{dim}}$ are dimensional inputs. The expected values are numerically integrated by means of either deterministic quadrature rules or nondeterministic MC techniques. Once again, the surrogate model obtained with the PCE is extremely useful to enhance computational performance:

$$(\nabla_{X_{\mathrm{dim}}} g)^T \frac{\partial \boldsymbol{X}_{\mathrm{dim}}}{\partial z} \approx (\nabla_{X_{\mathrm{dim}}} \hat{g})^T \frac{\partial \boldsymbol{X}_{\mathrm{dim}}}{\partial z} \tag{25}$$

If the problem of the increase in initial altitude is reconsidered, we obtain for the QB50 case study:

Table 7 Sobol indices for the QB50 case study[a]

Variable	Units
Drag correction	0.911
Initial altitude	0.022
Launch date	0.084
Initial RAAN	0.000

[a]These dimensionless indices indicate the contribution of each uncertainty source in the generation of the uncertainty in the orbital lifetime.

$$\frac{\partial \mu_Y}{\partial \mu_h} = 1.87 \frac{\text{day}}{\text{km}} \tag{26}$$

$$\frac{\partial \sigma_Y}{\partial \mu_h} = \frac{1}{2\sigma_Y}\frac{\partial \sigma_Y^2}{\partial \mu_h} = 0.86 \frac{\text{day}}{\text{km}} \tag{27}$$

Because the difference between the derivative of the mean and of the standard deviation is largely greater than zero, a small increase of the nominal initial altitude is a wise choice for an increase in lifetime. Indeed, for an arbitrary small variation of the nominal initial altitude $\delta\mu_H$, the lower 1-sigma confidence bound of the perturbed mean $\tilde{\mu}_Y - \tilde{\sigma}_Y$ is

$$\hat{\mu}_Y - \tilde{\sigma}_Y \approx \mu_Y - \sigma_Y + \underbrace{\left(\frac{\partial \mu_Y}{\partial \mu_h}\bigg|_{\mu_h} - \frac{\partial \sigma_Y}{\partial \mu_h}\bigg|_{\mu_h}\right)}_{>0}\delta\mu_h > \mu_Y - \sigma_Y \tag{28}$$

Because the PDF of the VOI is nonnormal, there is no point in generalizing Eq. (28) for larger intervals of confidence. For the analysis of different intervals of confidence, the CCDF is more adequate, which indicates the confidence at which the VOI is higher than a certain value. Figure 20 illustrates the CCDF for the nominal case and with a 1% perturbation of μ_H. Because the perturbed curve is always greater than the nominal curve, the applied perturbation is useful to efficiently increase the lifetime. However, this result cannot be generalized for any $\delta\mu_H$, and MC propagation of the perturbed set of uncertainty sources is mandatory to estimate the CCDF, unless an adequate labeled PDF is identified to represent the lifetime (e.g., with the maximum likelihood principle).

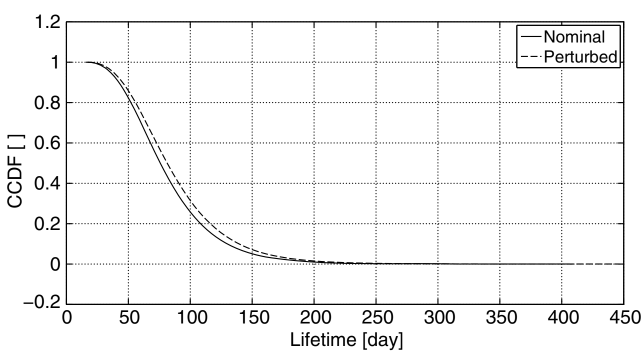

Fig. 20 CCDF of the orbital lifetime in nominal conditions and with a 1% perturbation on the nominal initial altitude.

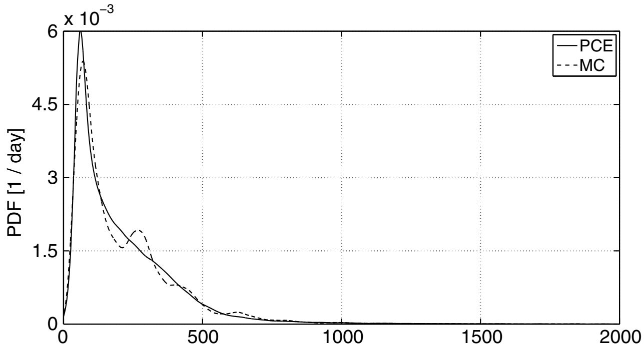

Fig. 21 PDF orbital lifetime of NanoSail-D2. MC propagation of the full set of uncertainties against PCE of the reduced set.

Table 8 Moments of the lifetime of NanoSail-D2[a]

	Reduced set (PCE), day	All variables (MC), day	Error, %
Mean	212.4	217.0	−2.1
Standard deviation	197.9	206.2	−4.0
$\sqrt[3]{\boldsymbol{M}_3}$	294.5	325.7	−9.6
$\sqrt[4]{\boldsymbol{M}_4}$	442.3	517.9	−14.6

[a]Error between the MC propagation with full set of uncertainty sources against PCE with the reduced set.

VII. Another Test Case: NanoSail-D2 Mission

A second test case, the deorbiting of the NanoSail-D2 spacecraft developed by NASA [44], is briefly discussed in this section. This spacecraft is a 4 kg three-unit CubeSat, the objective of which was to deploy in orbit a 10 m^2 solar sail. It was ejected from FASTSAT on 17 January 2011, and it deployed its sail three days later. Reentry happened on 17 September 2011 (i.e., after a 240 day lifetime).

Targeting the probabilistic assessment of the lifetime of NanoSail, a methodology similar to the one discussed in the present paper and in [11] is considered. We note that the attitude of this spacecraft is not controlled, which leads to a very wide distribution of the cross section. In addition, the initial orbital altitude is much larger (i.e., about 650 km). Because the full TLE data set was not available, the initial states were characterized according to the TLE measured right after the ejection. Intrinsic accuracy of the TLE was considered to characterize the covariance of the initial position [45].

The sensitivity analysis revealed that the drag correction factor was the only relevant uncertainty in the assessment of the uncertainty in the lifetime. With Sobol indices around 0.6 for both the daily and the averaged $F_{10.7}$, solar activity was found to be the variable responsible for most of the uncertainty in the drag correction factor. The Sobol index for the cross-sectional area was 0.08, whereas model error on the molecular nitrogen drastically dropped with respect to the QB50 case.

Because the drag correction factor is the dominant source of uncertainty, it results in a very efficient PCE-based propagation, because only eight evaluations of the VOI were necessary for a proper convergence of the surrogate model. The PDF given by PCE is compared with that of the full MC propagation in Fig. 21. The error between the moments of the two distributions are listed in Table 8. The agreement between the second-order descriptors is very satisfactory, which gives us further confidence in the proposed methodology and, in particular, in the reduction strategy. It is interesting to note that the lifetime of the actual mission (i.e., 240 days) is not far from the mean of the computed distribution. However, the loss of partial information in the definition of the drag correction factor is responsible for a smoothing of the distribution of the VOI (Fig. 21), which results in larger discrepancies in the higher order moments.

Finally, the large variability of the lifetime indicates that a purely ballistic deorbiting like in the NanoSail case is not an effective technique from the uncertainty point of view, because the adequate identification of a narrow reentry window is not possible. This result is supported by facts: the reentry of NanoSail was announced to happen on 29 November (i.e., 73 days after the experienced one; 30% error). The fact that the Sobol index of the cross section is relatively modest compared with the one of the solar weather proxies suggests that the variation in lifetime is more due to the long nominal mission lifetime, making it subject to large variations in the atmospheric environment, rather than to the sail itself. For this reason, similar results may be encountered for more traditional spacecraft with a similar nominal remaining lifetime.

Finally, we point out that this result depends on the particular mission window considered, which is limited to a quiet period of the solar cycle. Active periods are characterized by larger variability and uncertainty of the solar flux, so that, even if a smaller expected value of the lifetime occurred, the standard deviation to expected value ratio might also have been larger.

VIII. Conclusions

The focus of this paper was on propagation and sensitivity analysis of the uncertainties affecting the lifetime of an LEO object, whose remaining duration is on the order of a fraction of the solar cycle. Standard Monte Carlo propagation was found to be computationally intensive and was effectively replaced by polynomial chaos expansions. Because the cost of this latter method is intimately related to problem dimension, all the uncertainties affecting the drag force were condensed into a single random variable, which was termed the drag correction factor. In both case studies considered, the probability density function of orbital lifetime was characterized by a large standard deviation, which confirms that a deterministic assessment of lifetime should not be attempted. The subsequent sensitivity analysis revealed that the drag force, and, in particular, the drag correction factor, is by far the main contributor to lifetime variability.

Acknowledgments

Lamberto Dell'Elce would like to acknowledge the Belgian National Fund for Scientific Research for its financial support (Fonds pour la formation à la Recherche dans l'Industrie et dans l'Agriculture).This work was performed in the framework of the European Space Agency project "Uncertainty quantification for aerospace application" (grant manager: D. Giordano, European Space Agency; principal investigator: T. Magin, von Karman Institute for Fluid Dynamics).

References

[1] Junkins, J. L., Akella, M. R., and Alfriend, K. T., "Non-Gaussian Error Propagation in Orbital Mechanics," *Journal of Astronautical Sciences*, Vol. 44, No. 4, Oct.–Dec. 1996, pp. 541–563.

[2] Scheeres, D. J., Hsiao, F. Y., Park, R. S., Villac, B. F., and Maruskin, J. M., "Fundamental Limits on Spacecraft Orbit Uncertainty and Distribution Propagation," *Journal of Astronautical Sciences*, Vol. 54, Nos. 3–4, 2006, pp. 505–523. doi:10.1007/BF03256503

[3] Park, R. S., and Scheeres, D. J., "Nonlinear Mapping of Gaussian Statistics: Theory and Applications to Spacecraft Trajectory Design," *Journal of Guidance, Control, and Dynamics*, Vol. 29, No. 6, 2006, pp. 1367–1375. doi:10.2514/1.20177

[4] Giza, D., Singla, P., and Jah, M., "Approach for Nonlinear Uncertainty Propagation: Application to Orbital Mechanics," *Proceedings of the AIAA Guidance, Navigation, and Control Conference*, AIAA Paper 2009-6082, 2009.

[5] Fujimoto, K., Scheeres, D. J., and Alfriend, K. T., "Analytical Nonlinear Propagation of Uncertainty in the Two-Body Problem," *Journal of Guidance, Control, and Dynamics*, Vol. 35, No. 2, 2012, pp. 497–509. doi:10.2514/1.54385

[6] Robert, C. P., and Casella, G., *Monte Carlo Statistical Methods*, 2nd ed., Springer, Berlin, 2004, pp. 79–122.

[7] Jones, B. A., Doostan, A., and Born, G. H., "Nonlinear Propagation of Orbit Uncertainty Using Non-Intrusive Polynomial Chaos," *Journal of Guidance, Control, and Dynamics*, Vol. 36, No. 2, 2013, pp. 430–444. doi:10.2514/1.57599

[8] Jones, B. A., Doostan, A., and Born, G. H., "Conjunction Assessment Using Polynomial Chaos Expansions," *Proceedings of the 23rd International Symposium on Space Flight Dynamics*, Jet Propulsion Laboratory, Pasadena, CA, 2012.

[9] Jones, B. A., and Doostan, A., "Satellite Collision Probability Estimation Using Polynomial Chaos Expansions," *Advances in Space Research*, Vol. 52, No. 11, 2013, pp. 1860–1875. doi:10.1016/j.asr.2013.08.027

[10] Xiu, D., *Numerical Methods for Stochastic Computations: A Spectral Method Approach*, Princeton Univ. Press, Princeton, NJ, 2010, pp. 57–67.

[11] Dell'Elce, L., Arnst, M., and Kerschen, G., "Probabilistic Assessment of the Lifetime of Low-Earth-Orbit Spacecraft: Uncertainty Characterization," *Journal of Guidance, Control, and Dynamics*, May 2014, pp. 1–13. doi:10.2514/1.g000148

[12] Doornbos, E., *Thermospheric Density and Wind Determination from Satellite Dynamics*, Springer Theses, Springer, New York, 2012, pp. 17–80.

[13] Muylaert, J., Reinhard, R., Asma, C., Buchlin, J., Rambaud, P., and Vetrano, M., "QB50: An International Network of 50 Cubesats for Multi-Point, In-Situ Measurements in the Lower Thermosphere and for Re-Entry Research," *Proceedings of the ESA Atmospheric Science Conference*, ESA, Paris, 2009.

[14] Picone, J. M., Hedin, A. E., Drob, D. P., and Aikin, A. C., "NRLMSISE-00 Empirical Model of the Atmosphere: Statistical Comparisons and Scientific Issues," *Journal of Geophysical Research: Space Physics*, Vol. 107, No. A12, 2002, pp. SIA 15-1–SIA 15-16. doi:10.1029/2002JA009430

[15] Ashrafi, S., Roszman, L., and Cooley, J., "Nonlinear Techniques for Forecasting Solar Activity Directly from Its Time Series," *Proceedings of the Flight Mechanics/Estimation Theory Symposium*, NASA, Scientific and Technical Information Division, Washington, D.C., 1993, pp. 319–335.

[16] Watari, S., "Separation of Periodic, Chaotic, and Random Components in Solar Activity," *Journal of Solar Physics*, Vol. 168, No. 2, 1996, pp. 413–422. doi:10.1007/BF00148065

[17] Loskutov, A., Istomin, I. A., Kuzanyan, K. M., and Kotlyarov, O. L., "Testing and Forecasting the Time Series of the Solar Activity by Singular Spectrum Analysis," *Nonlinear Phenomena in Complex Systems*, Vol. 4, No. 1, 2001, pp. 47–57.

[18] Øksendal, B., *Stochastic Differential Equations: An Introduction with Applications*, 5th ed. Corrected Printing, Springer–Verlag, Heidelberg, Germany, 2003, pp. 1–6.

[19] Fraysse, H., Morand, V., Le Fevre, C., Deleflie, S., Wailliez, A., Lamy, A., Martin, T., and Perot, E., "Long Term Orbit Propagation Techniques Developed in the Frame of the French Space," *International Symposium on Space Flight Dynamics*, ESA, Paris, 2011, pp. 89–105.

[20] Woodburn, J., and Lynch, S., "Numerical Study of Orbit Lifetime," *Proceedings of the AAS/AIAA Astrodynamics Specialists Conference*, AAS Paper 2005-297, 2005.

[21] Eaton, M. L., *Multivariate Statistics: A Vector Space Approach*, Wiley, New York, 1983, pp. 103–131.

[22] Julier, S. J., and Uhlmann, J. K., "General Method for Approximating Nonlinear Transformations of Probability Distributions," Robotics Research Group, Dept. of Engineering Science, Univ. of Oxford, Technical Rept., Oxford, 1996.

[23] Cramér, H., *Mathematical Methods of Statistics*, Princeton Univ. Press, Princeton, NJ, 1997, pp. 341–415.

[24] Casella, G., and Berger, R., *Statistical Inference*, Duxbury, Pacific Grove, CA, 2002, pp. 207–270.

[25] Adams, B. M., Dalbay, K. R., Eldred, M. S., Swiler, L. P., Bohnhoff, W. J., Eddy, J. P., Vigil, D. M., Hough, P. D., and Lefantzi, S., "DAKOTA, A Multilevel Parallel Object-Oriented Framework for Design Optimization, Parameter Estimation, Uncertainty Quantification, and Sensitivity Analysis," Ver. 5.2, Reference Manual, Sandia National Lab., Livermore, CA, 2011.

[26] Rosenblatt, M., "Remarks on Some Nonparametric Estimates of a Density Function," *Annals of Mathematical Statistics*, Vol. 27, No. 3, 1956, pp. 832–837. doi:10.1214/aoms/1177728190

[27] Parzen, E., "On Estimation of a Probability Density Function and Mode," *Annals of Mathematical Statistics*, Vol. 33, No. 3, 1962, pp. 1065–1076. doi:10.1214/aoms/1177704472

[28] Sentman, L. H., "Free Molecule Flow Theory and Its Application to the Determination of Aerodynamic Forces," Lockheed Missiles and Space Co., Technical Rept. LMSC-448514, Sunnyvale, CA, 1961.

[29] Moe, K., and Moe, M. M., "Gas-Surface Interactions and Satellite Drag Coefficients," *Planetary and Space Science*, Vol. 53, No. 8, 2005, pp. 793–801. doi:10.1016/j.pss.2005.03.005

[30] Pilinski, M. D., Argrow, B. M., and Palo, S. E., "Semiempirical Model for Satellite Energy-Accommodation Coefficients," *Journal of*

Spacecraft and Rockets, Vol. 47, No. 6, 2010, pp. 951–956.
doi:10.2514/1.49330

[31] Ghanem, R., and Spanos, P., *Stochastic Finite Elements: A Spectral Approach*, Dover, New York, 2003, pp. 79–122.

[32] Le Maitre, O., and Knio, O., *Spectral Methods for Uncertainty Quantification: With Applications to Computational Fluid Dynamics*, Springer, New York, 2010, pp. 28–38.

[33] Doostan, A., and Iaccarino, G., "Least-Squares Approximation of Partial Differential Equations with High-Dimensional Random Inputs," *Journal of Computational Physics*, Vol. 228, No. 12, 2009, pp. 4332–4345.
doi:10.1016/j.jcp.2009.03.006

[34] Gentle, J. E., *Elements of Computational Statistics*, Springer, New York, 2002.

[35] Sobol, I., "Sensitivity Estimates for Non-Linear Mathematical Models," *Mathematical Modeling and Computational Experiments*, Vol. 1, No. 4, 1993, pp. 407–414.

[36] Saltelli, A., Ratto, M., Andres, T., Campolongo, F., Cariboni, J., Gatelli, D., Saisana, M., and Tarantola, S., *Global Sensitivity Analysis: The Primer*, Wiley, Hoboken, NJ, 2008, pp. 10–52.

[37] Sudret, B., "Global Sensitivity Analysis Using Polynomial Chaos Expansions," *Reliability Engineering and System Safety*, Vol. 93, No. 7, 2008, pp. 964–979.
doi:10.1016/j.ress.2007.04.002

[38] Saleh, J. H., Hastings, D. E., and Newman, D. J., "Spacecraft Design Lifetime," *Journal of Spacecraft and Rockets*, Vol. 39, No. 2, 2002, pp. 244–257.
doi:10.2514/2.3806

[39] Naasz, B. J., Berry, K., and Schatten, K., "Orbit Decay Prediction Sensitivity to Solar Flux Variations," *Proceedings of the AAS/AIAA Space Flight Mechanics Conference*, AAS Paper 2007-264, 2007.

[40] Moe, K., Moe, M. M., and Doornbos, E., "Outstanding Issues Related to Thermospheric Measurements and Modeling," *COSPAR Meeting*, Center of Applied Space Technology and Microgravity, 2010.

[41] Vallado, D. A., "Verifying Observational Data for Real-World Space Situational Awareness," *Proceedings of the AAS/AIAA Astrodynamics Specialist Conference*, AAS Paper 2011-439, 2011.

[42] Fu, M. C., "Gradient Estimation," *Handbooks in Operations Research and Management Science*, Vol. 13, Elsiever, Amsterdam, 2006, pp. 575–616.

[43] Crestaux, T., Le Maître, O., and Martinez, J. M., "Polynomial Chaos Expansion for Sensitivity Analysis," *Reliability Engineering and System Safety*, Vol. 94, No. 7, 2009, pp. 1161–1172.
doi:10.1016/j.ress.2008.10.008

[44] Johnson, L., Whorton, M., Heaton, A., Pinson, R., Laue, G., and Adams, C., "NanoSail-D: A Solar Sail Demonstration Mission," *Acta Astronautica*, Vol. 68, Nos. 5–6, 2011, pp. 571–575.
doi:10.1016/j.actaastro.2010.02.008

[45] Flohrer, T., Krag, H., and Klinkrad, H., "Assessment and Categorization of TLE Orbit Errors for the US SSN Catalogue," *Proceedings of the Advanced Maui Optical and Space Surveillance Technologies Conference*, Maui Economic Development Board, Inc., Kihei, HI, 2008.